



Comprehensive electrocatalytic degradation of tetracycline in wastewater by electrospun perovskite manganite nanoparticles supported on carbon nanofibers

Ziheng Li¹ · Wenhao Xie¹ · Feichong Yao^{1,5} · Ai Du² · Qiaoying Wang³ · Zhanhu Guo⁴ · Hongbo Gu¹

Received: 13 July 2022 / Revised: 27 July 2022 / Accepted: 29 August 2022 / Published online: 10 September 2022
© The Author(s), under exclusive licence to Springer Nature Switzerland AG 2022

Abstract

The perovskite manganite $\text{La}_{0.7}\text{Ca}_{0.3}\text{MnO}_3$ nanoparticle/carbon nanofiber (LCMO/CNF) nanocomposites are developed by annealing the electrospun polyvinylpyrrolidone (PVP) mixed with nitrates (manganous nitrate, lanthanum (III) nitrate, and calcium nitrate) to work as electrocatalysts for the degradation of tetracycline (TC). The results show that the LCMO/CNFs fabricated with annealing at 250 °C for 120 min in the air atmosphere and subsequent calcination at 650 °C for 60 min possess an outstanding TC degradation performance. The TC degradation percentage (DP%) could reach 94.0% for 10 mg L⁻¹ of TC solution with 0.1 mol L⁻¹ of Na₂SO₄ as supporting electrolyte within only 1 h at a bias voltage of 1.0 V (vs. SCE). The LCMO/CNF-modified electrode possesses an average power consumption of 5.41 kWh kg⁻¹ and the overall Faraday efficiency of 46.37% after 180 min of treatment, revealing a high efficiency and a relatively low cost. The TC DP% is changed from 87.8 to 84.8% after five cycles of electrocatalytic process for LCMO/CNF-modified electrode, implying an excellent durability, recyclability, and reusability. The TC degradation mechanism and pathways have also been explored. The results exhibit that the LCMO/CNFs could thoroughly electrocatalytically degrade TC into carbon dioxide and water at the end. This work provides a novel electrocatalyst for treatment of antibiotics contaminated wastewater with relatively low cost.

Keywords Perovskite manganite nanoparticles · Carbon nanofibers · Tetracycline · Electrocatalytic degradation · Mechanism

Ziheng Li and Wenhao Xie contributed equally to this work.

✉ Hongbo Gu
hongbogu2014@tongji.edu.cn

- ¹ Shanghai Key Lab of Chemical Assessment and Sustainability, School of Chemical Science and Engineering, Tongji University, Shanghai 200092, People's Republic of China
- ² Shanghai Key Laboratory of Special Artificial Microstructure Materials and Technology, School of Physics Science and Engineering, Tongji University, Shanghai 200092, People's Republic of China
- ³ State Key Laboratory of Pollution Control and Resource Reuse, College of Environmental Science and Engineering, Shanghai Institute of Pollution Control and Ecological Security, Tongji University, Shanghai 200092, China
- ⁴ Integrated Composites Lab (ICL), Department of Chemical & Biomolecular Engineering University of Tennessee, Knoxville, TN 37966, USA
- ⁵ College of Materials Science and Engineering, Taiyuan University of Science and Technology, Taiyuan 030024, People's Republic of China

1 Introduction

Even though the antibiotics are bacteriostatic and they could inhibit the synthesis of bacterial protein and kill the bacteria by blocking the enzymes [1, 2], the discharge of antibiotics into the water system could cause severe environmental problems since they could not be totally degraded by the environment itself [3–5]. Residues of antibiotics in the environment might result in the drug-resistance of human beings and create the superbugs [6]. Therefore, it is required to remove the antibiotics from the environment and water system [7, 8]. Compared with other methods like adsorption or photocatalysis, electrochemical process is recognized as an effective method for treatment of antibiotic pollutants with the advantages of high efficiency, simple operation, and thorough degradation without any secondary pollution [9]. However, its performance strongly depends on the electrode materials [10]. Therefore, it is demanded to develop

the novel catalytic materials with high efficiency for the degradation of antibiotics.

Recently, carbon nanocomposites containing multiple metals or metal oxides have been reported to act as the electrode materials for the degradation of antibiotics [11] since the carbon materials in the nanocomposites could promote the congregation and adsorption of antibiotics [12], and the metal or metal oxide supported on the carbon materials could serve as the active sites for effective electrocatalytic degradation of antibiotics [13]. For example, Liu et al. [14] coated nano antimony-doped tin dioxide (Sb-SnO₂) on a porous coal-based carbon membrane (CM) by the sol-gel method, which expressed an increased electrocatalytic degradation capability to the tetracycline (TC) compared with the pure CM. The TC removal rate by this membrane could still maintain 96.5% after 6 h of operation. Tang et al. [15] fabricated the molybdenum trioxide/nano-graphite (MoO₃/Nano-G) composites by a surfactant-assisted solvothermal method followed with low-temperature calcination, which could serve as the anodic catalysts for the electrocatalytic degradation of ceftazidime with a high efficiency of 99.9%. This result was much higher than that of nano-G (46.7%) and dimensionally stable anode (69.2%).

Perovskite manganites with the formula of R_{1-x}A_xMnO₃ (R = La and rare earths, A = Ca, Sr, Ba, etc.) could reveal the unique physical and chemical properties [16], further demonstrating the superb catalytic performance. Especially, as a member of perovskite manganites, the prototypical system of La_{1-x}Ca_xMnO₃ manganites could own many structural phases including canted antiferromagnetic (CAF), ferromagnetic (FM), paramagnetic (PM) phases, and other phases depending on the Ca-doped concentrations [17], which make them express the special physicochemical properties in the catalytic field. Nevertheless, there are few reports regarding La_{1-x}Ca_xMnO₃ on carbon material for the electrocatalytic degradation of antibiotics.

Based on the aforementioned, in this work, a novel electrocatalyst consisting of perovskite manganite La_{0.67}Ca_{0.33}MnO₃ nanoparticle/carbon nanofiber (LCMO/CNF) nanocomposite has been produced by calcination of electrospun polyvinylpyrrolidone (PVP)/nitrides (manganous nitrate, lanthanum (III) nitrate, and calcium nitrate) for the electrocatalytic oxidation of antibiotic TC. The optimal preparation conditions for manufacturing LCMO/CNFs with high TC degradation performance have been determined. The effects of parameters on the electrocatalytic degradation of TC by LCMO/CNF-modified electrode including bias voltage, pH value, and initial TC concentrations have been systematically studied. The TC degradation kinetics as well as possible degradation mechanism and pathways have been also explored. These LCMO/CNF nanocomposites reveal a prominent TC

degradation performance within 1 h with the low energy. This work provides a new insight for the efficiently electrocatalytic degradation of antibiotics in polluted wastewater.

2 Materials and methods

2.1 Materials

Tetracycline hydrochloride (C₂₂H₂₄N₂O₈·HCl, 97.5%) was bought from Shanghai Macklin Biochemical Co., Ltd. Polyvinylpyrrolidone (PVP, K30, Mw = 44,000 ~ 54,000), anhydrous ethanol (C₂H₅OH, 99.7%), sodium sulfate (Na₂SO₄, 99.0%), manganous nitrate solution (Mn(NO₃)₂, 49.0 ~ 51.0%), lanthanum (III) nitrate hexahydrate (La(NO₃)₃·6H₂O, 99%), calcium nitrate tetrahydrate (Ca(NO₃)₂·4H₂O), citric acid (C₆H₈O₇·H₂O, ≥ 99.5%), ammonia (NH₃·H₂O, 25 ~ 28 wt%), isopropanol (C₃H₇OH, ≥ 99.7%), and sulfuric acid (H₂SO₄, 95.0 ~ 98.0%) were supplied by Sinopharm Chemical Reagent Co., Ltd. All the chemicals were used as received without any further treatment.

2.2 Preparation of perovskite manganite La_{0.67}Ca_{0.33}MnO₃ (LCMO) nanoparticles on carbon nanofibers

First, the PVP (1.38 g) was dissolved in 4.0 mL of absolute ethanol under magnetic stirring. Simultaneously, the lanthanum (III) nitrate hexahydrate, calcium nitrate tetrahydrate, and manganous nitrate solution with a mole ratio of 2:1:3 were dissolved in 1.0 mL of absolute ethanol. Then, the mixed metal salt solution was added into the former PVP solution for 4 h of magnetic stirring at room temperature. Second, the well mixed PVP/nitrates solution was drawn into a 10.0 mL of syringe with a stainless-steel gauge needle (inner diameter of 0.70 mm). Afterwards, this syringe was put on an electrospinning instrument with a feed rate of 0.001 mm min⁻¹, an applied voltage of 20 kV, a tip-to-collector distance of 20 cm and collected on a roller receiver covered with aluminum foil to receive the electrospun PVP/nitrates nanofibers. Third, the PVP/nitrates nanofibers were dried in a vacuum oven for 12 h. Finally, the dried products were taken down from the aluminum foil and placed into a tube furnace (GSL-1100X-S, Kejing Co. Ltd., Hefei, China) and then annealed at 250 °C for 120 min with a heating rate of 2 °C min⁻¹ in the air atmosphere with the subsequence of 650 °C for 60 min under the same heating rate in the nitrogen condition at a flow rate of 20.0 mL min⁻¹ to attain the perovskite manganite La_{0.67}Ca_{0.33}MnO₃ (LCMO) nanoparticles on carbon nanofibers (LCMO/CNFs). This sample was indexed as LCMO/CNFs (250/120-650/60). The pure LCMO nanoparticles were also fabricated by sol-gel method for comparison. Please see details in the following part.

2.3 Preparation of $\text{La}_{0.67}\text{Ca}_{0.33}\text{MnO}_3$ (LCMO) nanoparticles by sol–gel method

The LCMO nanoparticles were also manufactured by sol-gel method. Briefly, the lanthanum (III) nitrate hexahydrate, calcium nitrate tetrahydrate, and manganous nitrate solution with a mole ratio of 2:1:3 were added into the 20 mL of deionized water for dissolution under the magnetic stirring. After that, the citric acid with 1.1 times mole of metal ions was put into the above solution and the solution was kept in a water bath at temperature of 60 °C. Then, the ammonia was added into the above solution dropwise until the pH was neutral. The magnetic stirring was continued at 60 °C for 4–6 h in the water bath until the solution became sol-gel. After that, the gel was put in a freeze-drier for 12 h and situated in an infrared tube furnace (Beijing Huace Testing Instrument Co., Ltd.) for self-ignition to obtain the precursor. Lastly, the precursor was ground in a mortar and pestle and placed in the tube furnace to calcinate at 650 °C for 10 h to obtain LCMO nanoparticles.

2.4 Characterizations

The microstructures of LCMO/CNFs were observed on a field emission scanning electron microscope (SEM, Hitachi S-4800 system) and a high-resolution transmission electron microscopy (HRTEM, Tecnai G2 F20, FEI Company). The crystalline structures of samples were captured by X-ray diffraction (XRD) analysis on a Bruker AXS D8 Advance X-ray diffractometer with a general area detector diffraction system (GADDS) in the range of 10 to 80°. X-ray photoelectron spectroscopy (XPS) analysis was carried out with a Thermo escalab 250Xi spectrometer with the excitation source of Al K ($h\nu = 1486.6$ eV) radiation at a power of 150 W. The deconvolution was conducted by the mixed Lorentzian-Gaussian (30% L/G) function for each fitting component after the Shirley type background subtraction.

2.5 Tetracycline electrocatalytic degradation evaluation by LCMO/CNF-modified electrode

About 5.0 mg of LCMO/CNFs samples were weighed by a microbalance (SQP, Sartorius) and uniformly attached to a Toray carbon paper (TGP-H-60) with a size of 2 × 4 cm by pressure through a conductive tape (PELCO Tabs™, Ted Pella, Inc.) with a diameter of 12 mm to construct a LCMO/CNF electrode. Each sample was weighed three times within a deviation of 1.0% to attain the average value.

The distinct TC concentrations were prepared by diluting 1.0 g L⁻¹ of TC stock solution with deionized water. The TC concentration mainly utilized in this work was 30.0 mg L⁻¹. A LCMO/CNF-modified electrode as the working electrode, a saturated calomel electrode (SCE) as the reference

electrode, and a platinum electrode as the counter electrode were connected with the electrochemical workstation (Shanghai Chenhua Instrument Co., Ltd.). A TC solution (20.0 mL) with the initial concentration of 30.0 mg L⁻¹ was placed in the electrolytic cell, and the electrocatalytic degradation was carried out in time–current mode under the bias voltage of 1.0 V (vs. SCE) at room temperature for 1 h. The TC concentrations in the solutions for all the experiments were measured by a high-performance liquid chromatography (HPLC, UltiMate3000, Thermo Fisher Scientific Inc.) with the rate of 0.800 mL min⁻¹, the column temperature of 30 °C, and the mobile phase of 25% methanol and 75% water at the wavelength of 356.5 nm. The gained standard TC concentration fitting curve with an equation of $A = 0.5308c$ is laid out in Fig. S1, where A is the peak area obtained from HPLC and c is the TC concentration. The reported value for each product was the average value of three measurements with a standard deviation within ± 1.0%. The degradation percentage (DP%) of TC was calculated by Eq. (1):

$$DP\% = \frac{c_0 - c_e}{c_0} \times 100 \quad (1)$$

where c_0 (mg L⁻¹) stood for initial TC concentration and c_e (mg L⁻¹) represented the final TC concentration in the solution after electrocatalytic degradation attained from HPLC results.

2.5.1 Optimal parameter exploration for synthesis of LCMO/CNFs with better tetracycline degradation performance

With the purpose of determining the optimal synthesis conditions for LCMO/CNFs with an excellent electrocatalytic performance, the different parameters including annealing temperature (600, 650, 700, and 750 °C, respectively), holding time (30, 60, 90, and 120 min, respectively) at 650 °C in the nitrogen condition and holding time (60, 90, 120, and 150 min) at 250 °C in the air atmosphere were exploited to produce the LCMO/CNFs. For adjudgment, the electrodes made from these different LCMO/CNFs were separately applied in the electrocatalytic degradation of 20.0 mL of TC solutions (30 mg L⁻¹) with the 0.1 mol L⁻¹ of supporting electrolyte Na₂SO₄ under the bias voltage of 1.0 V (vs. SCE) over the same treatment period of 1 h at room temperature to evaluate their electrocatalytic degradation capability. Hereafter, the solution was taken out for HPLC measurement.

2.5.2 Effect of bias voltage

The different bias voltages were applied in the electrochemical workstation to examine the effect of bias voltage on the

electrocatalytic degradation of TC solution (20 mL) with the initial TC concentration of 30 mg L^{-1} and 0.1 mol L^{-1} of Na_2SO_4 as supporting electrolyte at pH of 5.0 for 1 h by LCMO/CNF-modified electrode under the time-current mode.

2.5.3 Effect of pH value

The effect of pH value for solution on the electrocatalytic degradation of TC was investigated by choosing pH values of 3.0, 5.0, 7.0, 9.0, and 11.0 in 30.0 mg L^{-1} of TC solutions for 1 h under the bias voltage of 1.0 V (vs. SCE) by LCMO/CNF-modified electrode at room temperature. The pH value of TC solutions was adjusted by H_2SO_4 (1.0 mol L^{-1}) and NaOH (1.0 mol L^{-1}) with a pH meter (model: PHS-3E).

2.5.4 Effect of initial tetracycline concentration

The initial TC concentration effect on the electrocatalytic degradation of TC by LCMO/CNF-modified electrode was studied by treating TC solutions (20.0 mL) with an initial TC concentration of 10.0, 20.0, 30.0, 40.0, and 50.0 mg L^{-1} for 1 h at the bias voltage of 1.0 V (vs. SCE).

2.5.5 Kinetic study

In the kinetic study, the electrocatalytic degradation of TC was performed in the solution with an initial TC concentration of 30.0 mg L^{-1} at room temperature for different treatment periods of 20, 40, 60, 90, 120, 150, and 180 min.

2.5.6 Power consumption and Faraday efficiency analysis

The power consumption and Faraday efficiency in treatment periods of 20, 40, 60, 90, 120, 150, and 180 min were computed to evaluate the electrocatalytic efficiency of LCMO/CNF-modified electrode for the TC degradation.

2.5.7 Retention of LCMO/CNF-modified electrode

The LCMO/CNF-modified electrode was employed to perform the electrocatalytic degradation of TC solution (20.0 mL) with initial TC concentration of 30.0 mg L^{-1} for 1 h at room temperature. After electrocatalytic degradation, the solution was taken out for the residual TC concentration determination by HPLC. The used LCMO/CNF-modified electrode was washed by deionized water and this procedure was repeated for three times to make sure that there was no TC or intermediates left. Then, the above procedures were repeated with the regenerated LCMO/CNF-modified electrode for reuse. The retention was run for five times to explore the stability and reusability of LCMO/CNF-modified electrode.

2.5.8 Electrocatalytic degradation pathways of tetracycline by LCMO/CNF-modified electrode

The degradation products of TC solution with the initial TC concentration of 10.0 mg L^{-1} after 2 h of electrocatalytic degradation under the bias voltage of 1.0 V in the 0.1 mol L^{-1} of supporting electrolyte Na_2SO_4 were analyzed by HPLC. The 20.0 mL of TC solution with an initial TC concentration of 100.0 mg L^{-1} was electrocatalytically degraded for 3 h and then the solution was employed to detect the intermediates and products by the ultra performance liquid chromatography and quadrupole time of flight mass spectrometry (UPLC-MS, Acquity UPLC/UPC2/Xevo G2-XS QTOFMS, Waters Corporation) to predict the possible degradation pathways of TC by LCMO/CNF-modified electrode. The UPLC was recorded at 280 nm and the MS was performed in a positive ion mode. The total organic carbon (TOC) for 10 mg L^{-1} of TC solution before and after treatment was tested by a Shimadzu TOC-L analyzer.

3 Results and discussion

3.1 Structure characterization

The structures and morphologies of LCMO/CNFs annealed with the sequence of $250 \text{ }^\circ\text{C}$ for 120 min in the air atmosphere and $650 \text{ }^\circ\text{C}$ for 60 min in the nitrogen condition (LCMO/CNFs (250/120-650/60)) have been characterized by XRD, XPS, SEM and TEM. The XRD pattern of LCMO/CNFs (250/120-650/60) is shown in Fig. 1a. The diffraction peaks located at 23.0 , 32.8 , 40.5 , 47.1 , 58.5 , 68.7 , and 78.3° are associated with (1 1 0), (1 1 2), (0 2 2), (0 0 4), (1 3 2), (2 2 4), and (1 1 6) crystallographic planes of $\text{La}_{0.67}\text{Ca}_{0.33}\text{MnO}_3$ (JCPDS No. 87-1084) [18], connoting the existence of perovskite manganite $\text{La}_{0.67}\text{Ca}_{0.33}\text{MnO}_3$ nanoparticles in the LCMO/CNFs (250/120-650/60). The element compositions and chemical states of LCMO/CNFs (250/120-650/60) have been conducted on XPS. The C 1s high-resolution XPS spectrum of LCMO/CNFs (250/120-650/60), Fig. 1b, is deconvoluted into four peaks at 283.8, 284.6, 285.7, and 288.4 eV, according with C-C, C-H, C-N, and C=O, respectively [19]. Figure 1c gives the high-resolution XPS spectrum of La 3d, which confirms the presence of La(II) and La(III). The peaks at 831.8 and 848.9 eV are assigned to La $3d_{5/2}$ and La $3d_{3/2}$ of La(II), accordingly. The peaks centered at 835.5 and 852.7 eV belong to La $3d_{5/2}$ and La $3d_{3/2}$ of La(III), respectively [20]. In Fig. 1d, the binding energy peaks in the high-resolution XPS spectrum of Ca 2p at 344.2 and 347.9 eV are respectively attributed to Ca $2p_{3/2}$ and Ca $2p_{1/2}$ [21]. Figure 1e provides the high-resolution

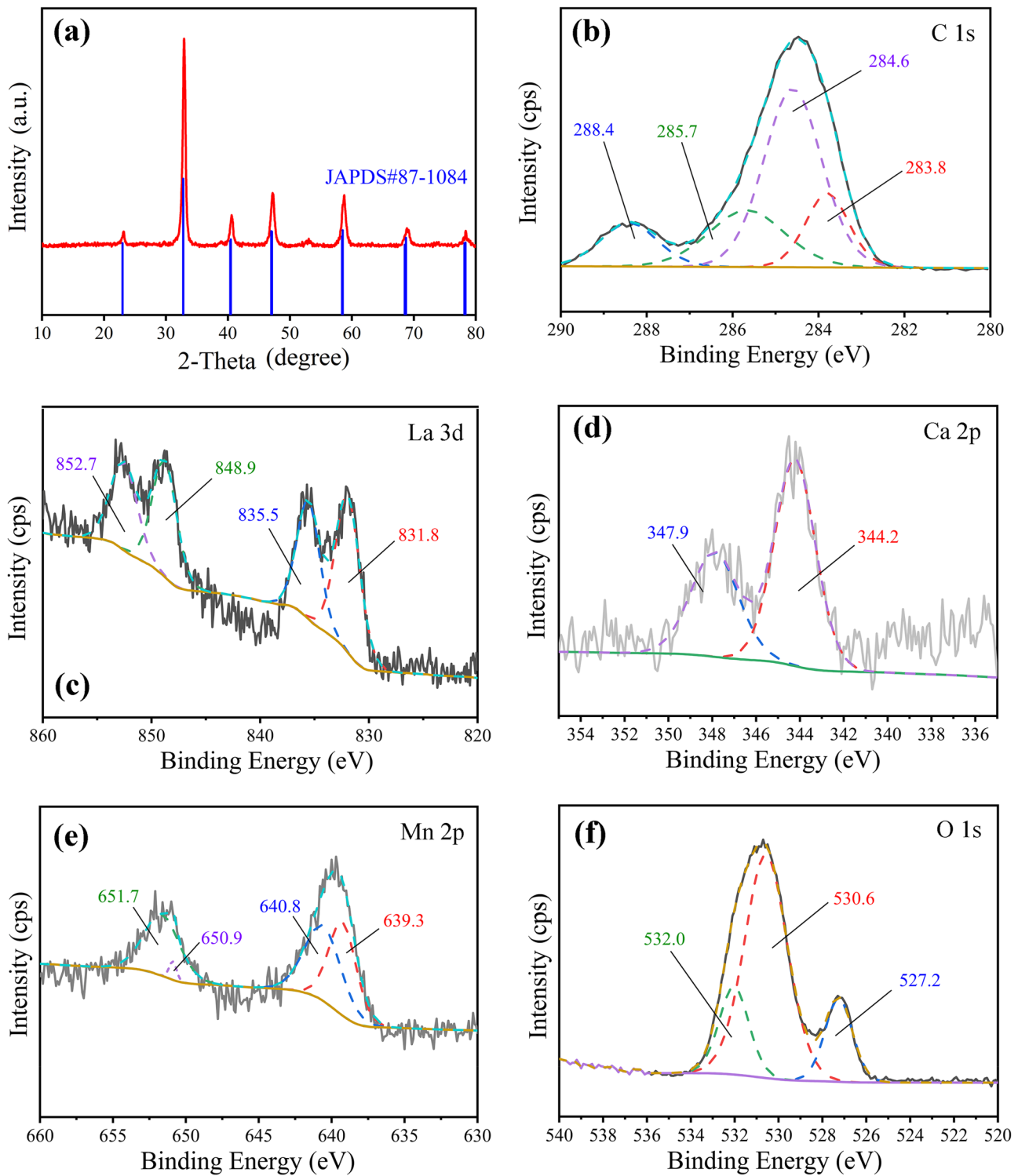


Fig. 1 a XRD pattern; high-resolution XPS spectra of b C 1s, c La 3d, d Ca 2p, e Mn 2p, and f O 1s for LCMO/CNFs nanocomposites annealed at 650 °C for keeping 60 min

XPS spectrum of Mn 2p, in which there are two chemical valences including Mn(III) and Mn(IV). The fitting peaks at 639.3 and 650.9 eV are contributed to the Mn $2p_{3/2}$ and Mn

$2p_{1/2}$ of Mn(III), respectively. The binding energy peaks at 640.8 and 651.7 eV are ascribed to Mn $2p_{3/2}$ and Mn $2p_{1/2}$ of Mn(IV), respectively [22]. The high-resolution

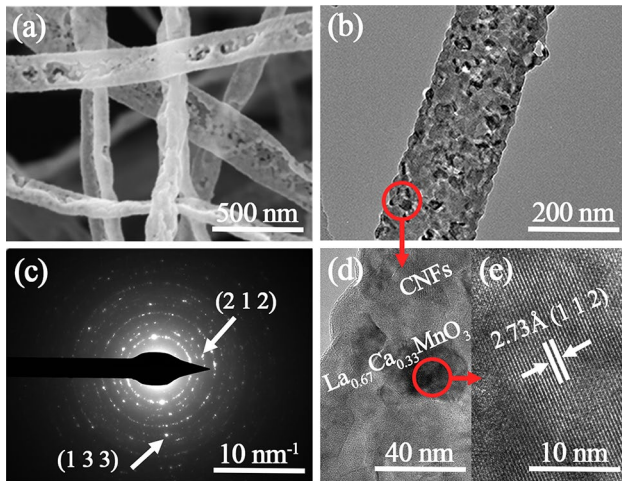


Fig. 2 **A** SEM image; **B** TEM image; **C** and **D** high resolution TEM (HRTEM) image of LCMO/CNFs; **E** selected area electron diffraction (SAED) of $\text{La}_{0.67}\text{Ca}_{0.33}\text{MnO}_3$ nanoparticles

XPS spectrum of O 1s is displayed in Fig. 1f. It is found to be deconvoluted into three peaks at 527.2, 530.6, and 532.0 eV, which are assigned to O^{2-} , O^- and carbonyl species, respectively [23]. These results confirm the composition and complex chemical states of elements for $\text{La}_{0.67}\text{Ca}_{0.33}\text{MnO}_3$ nanoparticles.

Figure 2a supplies the SEM image of LCMO/CNFs (250/120-650/60), which depicts the typical fibrous morphology with the average diameter of ~ 200 nm measured by Nano Measure software 2.0. The internal microstructures of LCMO/CNFs (250/120-650/60) are further verified by TEM and HRTEM images (Fig. 2b, d, and e, respectively), illustrating that the framework of LCMO/CNFs (250/120-650/60) is constructed from the nanofibers by amorphous carbon and the crystallized nanoparticles are distributed on the surface as well as inside of CNFs, Fig. 2d. In the crystallized region, as exhibited in Fig. 2e, the calculated lattice distance of 0.273 nm agrees well with the (1 1 2) crystallographic plane of $\text{La}_{0.67}\text{Ca}_{0.33}\text{MnO}_3$ in the light

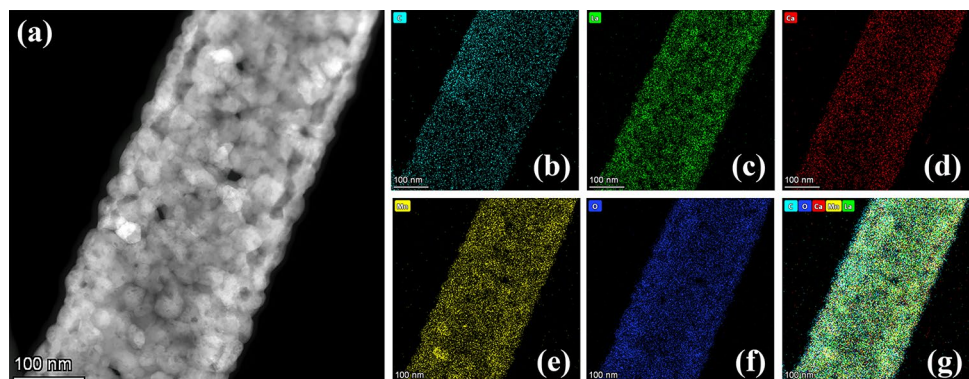
of JCPDS No. 87-1084. Figure 2c sets out the selected-area electron diffraction (SAED) for the crystallized nanoparticles in the LCMO/CNFs (250/120-650/60). It is noted that the calculated lattice distances of 0.208 and 0.143 nm from the diffraction patterns coincide with the (2 1 2) and (1 3 3) crystallographic planes of $\text{La}_{0.67}\text{Ca}_{0.33}\text{MnO}_3$ (JCPDS No. 87-1084). These results accord with the results of XRD analysis.

Figure 3 gives the elemental mapping from the energy filtered TEM (EFTEM) for a single LCMO/CNFs (250/120-650/60) nanofiber. It is worth mentioning that the elements of La, Ca, Mn, and O are uniformly dispersed on the framework of carbon nanofibers (C element). Based on the above results, it concludes that the LCMO/CNFs are created from the crystallized $\text{La}_{0.67}\text{Ca}_{0.33}\text{MnO}_3$ nanoparticles in situ grown on the amorphous CNFs.

3.2 Optimization of LCMO/CNFs structure with a better tetracycline degradation performance

With the aim to attain a better TC degradation performance, the optimum conditions for fabricating LCMO/CNFs have been determined. The different annealing temperatures (600, 650, 700, and 750 °C) and different holding time (30, 60, 90, and 120 min) at 650 °C in the nitrogen condition as well as different holding time (60, 90, 120, and 150 min) at 250 °C in the air atmosphere were picked out for outputting the LCMO/CNF samples. The SEM and XRD results for these LCMO/CNF samples are listed in Figs. S4, S5, and S6, and Fig. 4A, C, and E, respectively. The DP% of TC has been considered a judge for the optimal factors to produce the LCMO/CNFs. After treating 30 mg L^{-1} of TC solution in the 0.1 mol L^{-1} supporting electrolyte of Na_2SO_4 with LCMO/CNF-modified electrode for 1 h at the bias voltage of 1.0 V (vs. SCE), the acquired DP% results are drawn in Fig. 4B, D, and F. As shown in Fig. S4, it is found that all the LCMO/CNF samples prepared under the different annealing temperatures (600, 650, 700, and 750 °C)

Fig. 3 EFTEM of LCMO/CNFs: **A** zero-loss image; **B** C mapping; **C** La mapping; **D** Ca mapping; **E** Mn mapping; **F** O mapping; and **G** C + O + Ca + Mn + La mapping



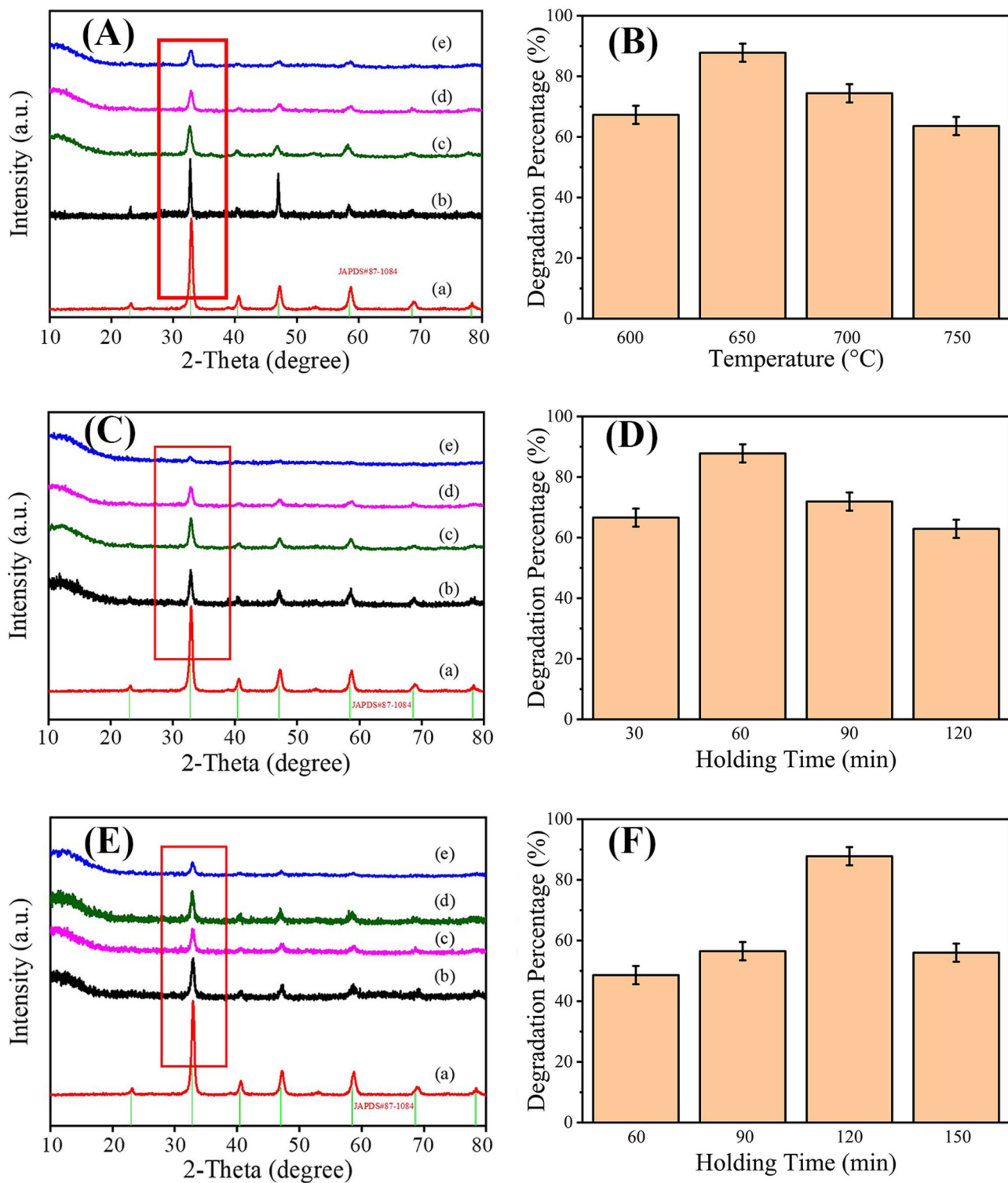


Fig. 4 A XRD patterns of (a) LCMO nanoparticles fabricated by sol-gel method; LCMO/CNFs prepared at annealing temperatures of (b) 750, (c) 700, (d) 650, and 600 °C; B corresponding TC DP% of LCMO/CNFs prepared at different annealing temperatures; C XRD patterns of (a) LCMO nanoparticles fabricated by sol-gel method; LCMO/CNFs prepared at holding time of (b) 120, (c) 90, (d) 60, and 30 min at 650 °C in the nitrogen condition; D corresponding TC DP%

of LCMO/CNFs prepared at different holding time at 650 °C in the nitrogen condition; E XRD patterns of (a) LCMO nanoparticles fabricated by sol-gel method; LCMO/CNFs prepared at holding time of (b) 150, (c) 120, (d) 90, and (e) 60 min at 250 °C in the air; F corresponding TC DP% of LCMO/CNFs prepared at different holding time at 250 °C in the air

reveal the fibrous morphology, whereas their surface structures vary at the different annealing temperatures. With the increasing annealing temperature from 600 to 750 °C in the nitrogen condition, the nanoparticles on the surface of LCMO/CNF samples become obvious. Especially, at temperature of 750 °C, numerous nanoparticles appear on the surface of LCMO/CNFs and a lot of holes are formed within the whole fibrous structure. This may be the reason that the high temperature accelerates the degradation of PVP polymer and the decreased carbon content induces the contact of more metal salts in the PVP polymer, leading to the formation of LCMO nanoparticles in the solid phase reaction [24]. This could also be affirmed by XRD results in Fig. 4B. On the contrary, the LCMO nanoparticles prepared by sol-gel method exhibit the particulate morphology with the average diameter of ~40 nm measured by Nano Measure software 2.0 in Fig. S7. Figure 4A manifests the XRD pattern of LCMO nanoparticles prepared by sol-gel method (Fig. 4A-a) and LCMO/CNFs produced under the different annealing temperatures (Fig. 4A-b–e). It is noticed that the XRD pattern of all the LCMO/CNFs is similar to that of LCMO nanoparticles prepared by sol-gel method, which is consistent with the crystallographic planes of $\text{La}_{0.67}\text{Ca}_{0.33}\text{MnO}_3$ (JCPDS No. 87-1084). However, with increasing annealing temperature, the diffraction peaks of LCMO/CNFs become evident and sharp. The TC degradation results in Fig. 4B express that the LCMO/CNFs do possess the electrocatalytic capability for TC degradation and the LCMO/CNFs manufactured under the annealing temperature of 600, 650, 700, and 750 °C indicate the TC DP% values of 67.1, 87.8, 73.6, and 63.2%, respectively. The highest DP% of TC is observed in the LCMO/CNF sample prepared at annealing temperature of 650 °C, which implies that 650 °C is the appropriate annealing temperature for fabricating LCMO/CNFs with the better TC degradation performance. As the holding time during annealing process is changed from 30 to 120 min at 650 °C in the nitrogen condition, as shown in SEM images of Fig. S5a–h, the degradation of LCMO/CNFs is deepened and the clear break occurs in the LCMO/CNF nanofibers, especially for the sample for the holding time of 120 min, Fig. S5g and h. In the XRD pattern of Fig. 4C, as the holding time is 30 min, the LCMO/CNF sample has no obvious diffraction peaks of LCMO nanoparticles, Fig. 4C-e. With the prolongation of holding time to 60 min, the diffraction peaks for LCMO nanoparticles emerge, Fig. 4C-d. After further increasing the holding time to 90 and 120 min, the intensity of diffractions peaks for LCMO nanoparticles becomes stronger. The DP% of TC for the LCMO/CNFs prepared under the holding time of 30, 60, 90, and 120 min at 650 °C in the nitrogen condition is 66.6, 87.8, 71.9, and 62.9%, respectively. This suggests that the extension of holding time could facilitate the formation of LCMO nanoparticles during the solid phase reaction, but it may decrease the

DP% of TC by LCMO/CNFs. Therefore, the holding time of 60 min at 650 °C in the nitrogen condition is suitable for manufacturing LCMO/CNFs with the better TC degradation performance. During the annealing process, we have found that the LCMO/CNFs could not be manufactured if there is no annealing process at 250 °C in the air atmosphere. Hence, afterwards, we have studied the holding time (60, 90, 120, and 150 min) at 250 °C in the air atmosphere to produce the LCMO/CNFs. As depicted in SEM images of Fig. S6, it is clear that as the holding time is altered from 60 to 120 min, the LCMO/CNFs could still well maintain the fibrous morphology. However, when the holding time is extended to 150 min, the morphology of LCMO/CNFs becomes curved and the nanoparticles turn into evidence. The DP% of TC by LCMO/CNFs synthesized at 250 °C in the air atmosphere under the holding time of 60, 90, 120, and 150 min is 48.6, 56.5, 87.8, and 56.0%, respectively. This means that the holding time of 120 min at 250 °C in the air atmosphere is favorable for the production of LCMO/CNFs with the better TC degradation performance.

In a word, the optimal preparation conditions of LCMO/CNFs with a better TC degradation performance are that the electrospun PVP/nitrides nanofibers are annealed at 250 °C for 120 min in the air atmosphere and then calcined at 650 °C for 60 min in the nitrogen condition. This sample is recognized as LCMO/CNFs (250/120-659/60), which could obtain the 87.8% of TC degradation as aforementioned. By contrast, the LCMO nanoparticles fabricated by sol-gel method (SEM image in Fig. S7) only exhibit 75.1% of TC degradation in the same treatment condition (20 mL of 30 mg L⁻¹ TC solution with 0.1 mol L⁻¹ Na₂SO₄ for 1 h treatment of electrocatalytic degradation). This verifies the superiority of our LCMO/CNFs. The samples exploited in the following experiments are LCMO/CNFs (250/120-650/60) and we have applied LCMO/CNFs instead for easy expression.

3.3 Determination of tetracycline electrocatalytic degradation

The effect of factors including bias voltage, pH value of the solution, and initial TC concentration on the TC electrocatalytic degradation by LCMO/CNF-modified electrode has been systematically assessed. First, the results for the effect of bias voltage on the TC degradation have been studied in the 30 mg L⁻¹ of TC solution with 0.1 mol L⁻¹ of Na₂SO₄ at the bias voltage values of 0.6, 0.8, 1.0, and 1.1 V (vs. SCE) for 1 h as shown in Fig. 5A. The DP% of TC for the bias voltage values of 0.6, 0.8, 1.0, and 1.1 V (vs. SCE) by LCMO/CNF-modified electrode is 30.7, 66.0, 87.8, and 91.4%, respectively. It is evident that the DP% of TC by LCMO/CNF-modified electrode is raised with increasing the bias voltage. However, as the bias voltage comes to 1.1 V (vs. SCE), many bubbles appear on the surface of anode since this value is close to the theoretical water splitting

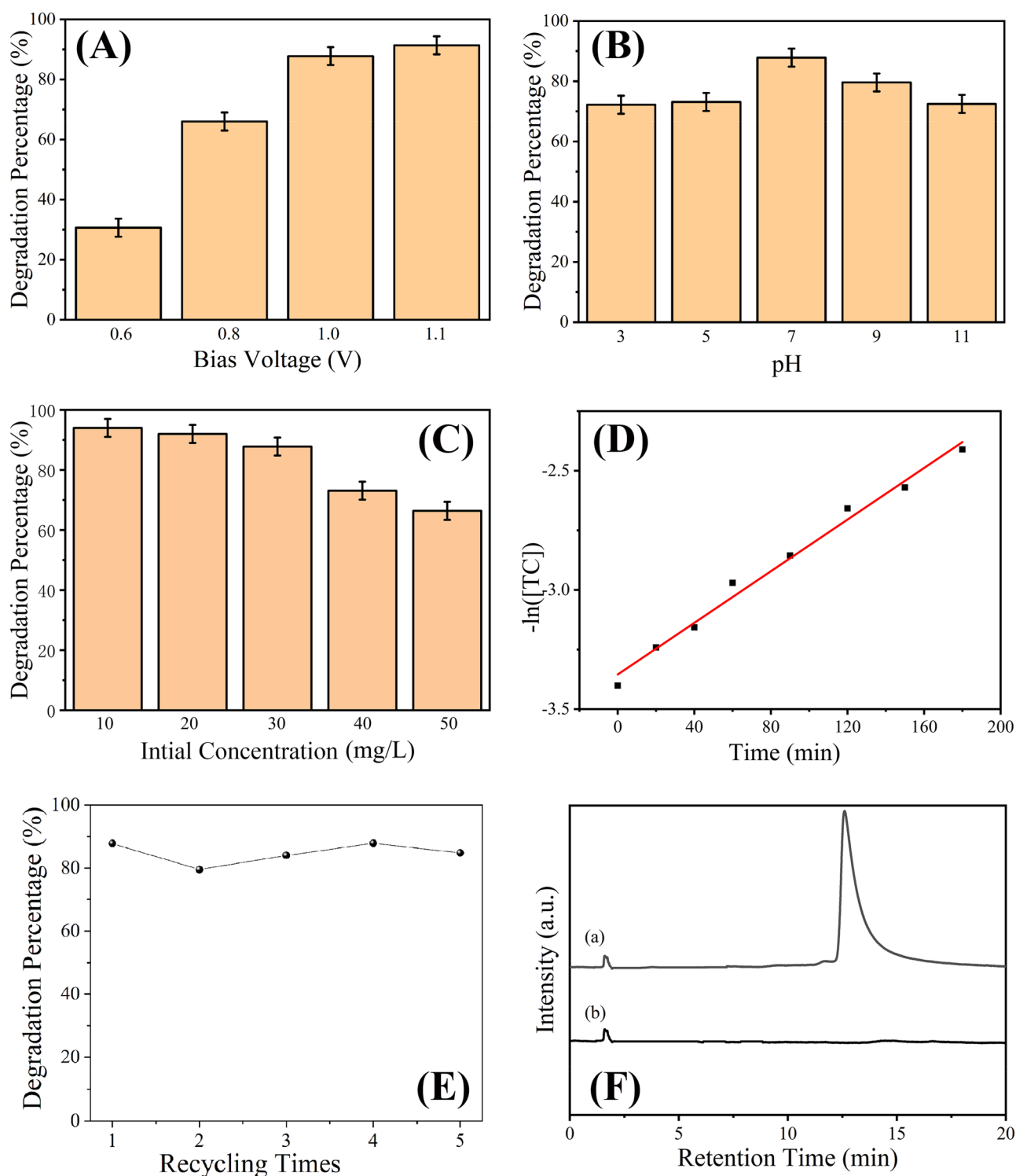


Fig. 5 **A** DP% in the TC solutions (20 mL, 30 mg L⁻¹) at different bias voltages catalyzed by LCMO/CNFs for 1 h at room temperature; **B** effect of different pH values on the DP% of TC solution (20 mL, 30 mg L⁻¹, with 0.1 M Na₂SO₄) at 1.0 V (vs. SCE) for 1 h at room temperature; **C** DP% in 20 mL of TC solutions with different initial TC concentrations catalyzed at 1.0 V for 1 h at room temperature;

D kinetic plot during the treatment of 20.0 mL TC solution (initial concentration of 30 mg L⁻¹) within 180 min at room temperature; **E** DP% of TC solutions (20 mL, 30 mg L⁻¹) at 1.0 V (vs. SCE) for 1 h catalyzed by recycled LCMO/CNFs at room temperature; **F** HPLC of (a) the solution electrocatalyzed by LCMO/CNFs after 12 h and (b) blank

voltage of 1.23 V and the oxygen evolution reaction starts. The gas evolution would hinder the TC degradation, further impairing the stability of electrode [14]. Consequently, the following experiments have been performed at the bias voltage of 1.0 V (vs. SCE).

The effect of pH value for solution on the TC degradation by LCMO/CNFs has also been investigated in 30 mg L⁻¹ of TC solution with the pH value from 3.0 to 11.0 for 1 h at the bias voltage of 1.0 V (vs. SCE) and the results are displayed in Fig. 5B. It comes out that the DP% of TC in the solution with pH values of 3.0, 5.0, 7.0, 9.0, and 11.0 by LCMO/CNFs is 72.2, 73.1, 87.8, 79.6, and 72.5%, respectively. Undoubtedly, the TC degradation performance by LCMO/CNF-modified electrode reaches the best value in the solution with pH value of 5.0. This result is also observed in the Fe-Co/carbon nanofibers [25] because the existing forms of TC in the solution are strongly dependent on the pH value of solution.

Figure 5C provides the effect of different initial TC concentrations such as 10, 20, 30, 40, and 50 mg L⁻¹ on the TC degradation by LCMO/CNF-modified electrode for 1 h at the bias voltage of 1.0 V (vs. SCE). The DP% of TC for the solution with initial TC concentration of 10, 20, 30, 40, and 50 mg L⁻¹ is 94.0, 92.0, 87.8, 73.1, and 67.2%, separately. It is found that the TC degradation performance by LCMO/CNF-modified electrode is declined as the initial TC concentration raises. It is reported that with increasing the initial TC concentration, the more TC molecules and intermediates would compete for the limited catalytic sites [26], which is not beneficial for the TC degradation on the electrode and causes the decreased TC degradation performance.

Later on, the kinetics of TC degradation by LCMO/CNF-modified electrode is examined through the TC concentration (c_t)~reaction time (t) plot by treating 50 mL of TC solution (30 mg L⁻¹) with 0.1 mol L⁻¹ of supporting electrolyte Na₂SO₄ at bias voltage of 1.0 V (vs. SCE), and the obtained results are depicted in Fig. S9. It shows that the c_t is decreased with increasing t . The c_t is declined quickly at the beginning and then decreased slowly. The pseudo-first-order reaction kinetics is introduced to describe the kinetics as Eq. (2):

$$\ln[c_t] = \ln[c_0] - kt \quad (2)$$

where c_0 (mg L⁻¹) is the initial TC concentration, c_t (mg L⁻¹) represents the TC concentration within time t and k stands for the pseudo-first-order rate constant. After fitting, the result is laid out in Fig. 5D. It is noted that the plot $\ln[c_t] \sim t$ is well linearly fitted with the pseudo-first-order kinetic model with a correlated coefficient of $r^2 = 0.993$. The calculated degradation rate constant k from the intercept ($1/k$) of the linear plot of $\ln[c_t] \sim t$ is 0.00541 min⁻¹ at the bias voltage of 1.0 V (vs. SCE) with current lower than 1 mA.

In common electrocatalytic degradation process, high energy consumption is always a large disadvantage. To

measure the energy efficiency during the electrocatalytic degradation of TC by LCMO/CNF-modified electrode, the power consumption has been estimated by Eq. (S1) and the Faraday efficiency has been figured out by Eq. (S2), as shown in Fig. S10. In the very first 2 h, the electrocatalytic degradation process exhibits a high Faraday efficiency up to 98.29% and a low power consumption of 2.55 kWh kg⁻¹. However, the Faraday efficiency is decreased when the electrocatalysis time is extended since more energy is consumed in the process of mass transfer as the TC concentration is decreased. In the end, an overall Faraday efficiency of 46.37% is obtained after 180 min of treatment, which is much higher than that of Fe/Co-CNFs (26.13%) [25]. On the contrary, the power consumption is increased in a long-term treatment and the average power consumption is calculated to be 5.41 kWh kg⁻¹, which is much lower than that of Fe/Co-CNFs (19.2 kWh kg⁻¹). When the price of industrial electricity in Shanghai is regarded as 0.65 CNY per kWh, the cost for the electrocatalytic degradation of 1 kg TC by LCMO/CNF-modified electrode is about 3.52 CNY.

The stability and recyclability of LCMO/CNF-modified electrode are identified by reusing the same electrode for the electrocatalytic degradation of TC solution (30 mg L⁻¹) for 1 h at the bias voltage of 1.0 V (vs. SCE). As is shown in Fig. 5E, the DP% of TC for the 1st and 5th is 87.8% and 84.8%, respectively, suggesting an excellent stability and reusability of LCMO/CNF-modified electrode.

In summary, the as-prepared LCMO/CNF-modified electrode discloses an outstanding electrocatalytic performance for the TC degradation and it could quickly realize the TC degradation with 1 h. In comparison, the published literature on the TC treatment is listed in Table 1. The results show that our LCMO/CNFs own a greater electrocatalytic degradation ability for TC and a relatively lower treatment time (1 h) than other materials in literature, which could effectively cut down the energy consumption and treating cost. As a result, it was proposed that as-prepared LCMO/CNFs have a great potential for the TC degradation with relatively low cost.

3.4 Possible tetracycline degradation mechanism and pathway exploration

The possible TC degradation mechanism by LCMO/CNFs has been explored. It is reported that there are two reaction modes including direct and indirect degradations for electrochemical degradation of organic pollutants, which are taken place directly at the surface of anode or through the mediation of oxidizer generated at the anode like hydroxyl radicals, respectively [27]. In this work, we have applied isopropanol to serve as the quencher for the hydroxyl radical to see if it could hinder the interaction between TC and

Table 1 Comparison on the TC treatment in literature

Materials	Technologies	Initial TC concentration (mg L ⁻¹)	Reaction conditions	Removal effect of tetracycline
Bi-Sn-Sb/ γ -Al ₂ O ₃ three-dimensional particle electrode [29]	Electrocatalysis	100	Current intensity of 0.1 A	Removal rate of 85.9% within 3 h
Iron/cobalt alloy nanoparticles on carbon nanofibers [25]	Electrocatalysis	30	Bias voltage of 1 V	Removal rate of 100% within 12 h
Hexagonal S-scheme AgBr/Zn-Al mixed metal oxides [30]	Photocatalysis	10	Visible light with incident intensity of 10 mW cm ⁻²	Removal rate of 95% within 1 h
TiO ₂ doped with acetylene black [31]	Photocatalysis	30	Visible light with incident intensity of 50 W m ⁻² , 3 mmol L ⁻¹ of persulfate	Removal rate of 93.3% within 2 h
Dual Z-scheme bismuthzirconate/graphitic carbon nitride/silver phosphate [32]	Photocatalysis	20	Visible light with wavelength > 420 nm by a 300 W Xenon lamp	Removal rate of 86.2% within 45 min
Cu-doped Fe@Fe ₂ O ₃ core-shell nanoparticles loaded on the nickel foam [33]	Heterogeneous electro-Fenton process	20	Current density of 40 mA cm ⁻² , air flow rate of 0.1 L min ⁻¹ , shaking speed of 400 rpm	Removal rate of 98.1% within 2 h
Fe/Ni bimetallic nanoparticles [34]	Redox reaction	100	Shaking speed of 250 rpm	Removal rate over 90% within 3 h
LCMO/CNFs In this work	Electrocatalysis	10	Bias voltage of 1 V	Removal rate of 94.0% within 1 h

hydroxyl radical. We have put 1 mol L⁻¹ of isopropanol into TC solution, and the DP% of TC is declined markedly from 87.8 to 64.6%. This recommends that the hydroxyl radical is a crucial mediator during the electrocatalytic degradation process of TC on the LCMO/CNF-modified electrode, meaning that the TC degradation by LCMO/CNFs is an indirect process.

The possible TC degradation pathways by LCMO/CNF-modified electrode have been also studied. We have utilized the LCMO/CNF-modified electrode to treat 20 mL of 10 mg L⁻¹ of TC solution with 0.1 mol L⁻¹ of supporting electrolyte Na₂SO₄ solution for 12 h and the HPLC results have indicated that there is no obvious peak around 12.7 min existed, Fig. 5F- b, (in Fig. 5F-a, in the HPLC curve of the original solution, it has an apparent TC peak at about 12.7 min), demonstrating that the TC has been totally electrocatalyzed by the LCMO/CNF-modified electrode into carbon dioxide and water. We have also exploited the TOC tests to verify this result. The TOC of solution before treatment is 43.86 mg L⁻¹ and becomes 0.71 mg L⁻¹ after treatment, which is much close to that of deionized water (0.62 mg L⁻¹). These results illustrate that the final products of TC in the solution after electrocatalytic degradation by LCMO/CNFs are carbon dioxide and water.

With the purpose of examining the degradation pathways of TC during the electrocatalytic process by LCMO/CNF-modified electrode, the products or intermediates after 3 h

electrocatalytic degradation of 20 mL TC solution with initial concentration of 100 mg L⁻¹ under 1.0 V (vs. SCE) are detected by UPLC-MS, and the gained chromatogram results are displayed in Fig. S11. It is found that the main peak with m/z = 445.16 in the base peak chromatogram (BPC) of solution is assigned to the TC molecule. There are many other peaks present in the BPC of degraded solution, denoting the intermediates during the electrocatalytic process. Relating to the results of MS spectra, the molecules corresponding to these peaks have been identified and the results are listed in Table S1. As a consequence, the possible pathways for the electrocatalytic degradation of TC by LCMO/CNF-modified electrode are provided in Fig. 6. In the molecule of TC, there are various manifold ionizable functional groups or electron-rich groups, such as dimethyl amino group, phenolic group, and conjugated double bond. These groups are easy to be attacked by hydroxyl radicals, which leads to the formation of different products [28]. As seen in P1 and P2, the double bonds in different ring structures are orderly attacked by hydroxyl radicals; meanwhile, the hydroxyl groups nearby are oxidized into carbonyl groups. Then a gradual demethylation process is conducted, when the dimethylamino group in P1 or P6 is completely removed and P9 comes into being. In P8, most of the functional groups have been removed after the dehydration and demethylation processes. Finally, ring structures open because of the attack of hydroxyl radicals, as displayed in P10. Furthermore, P11 and P12 indicate the

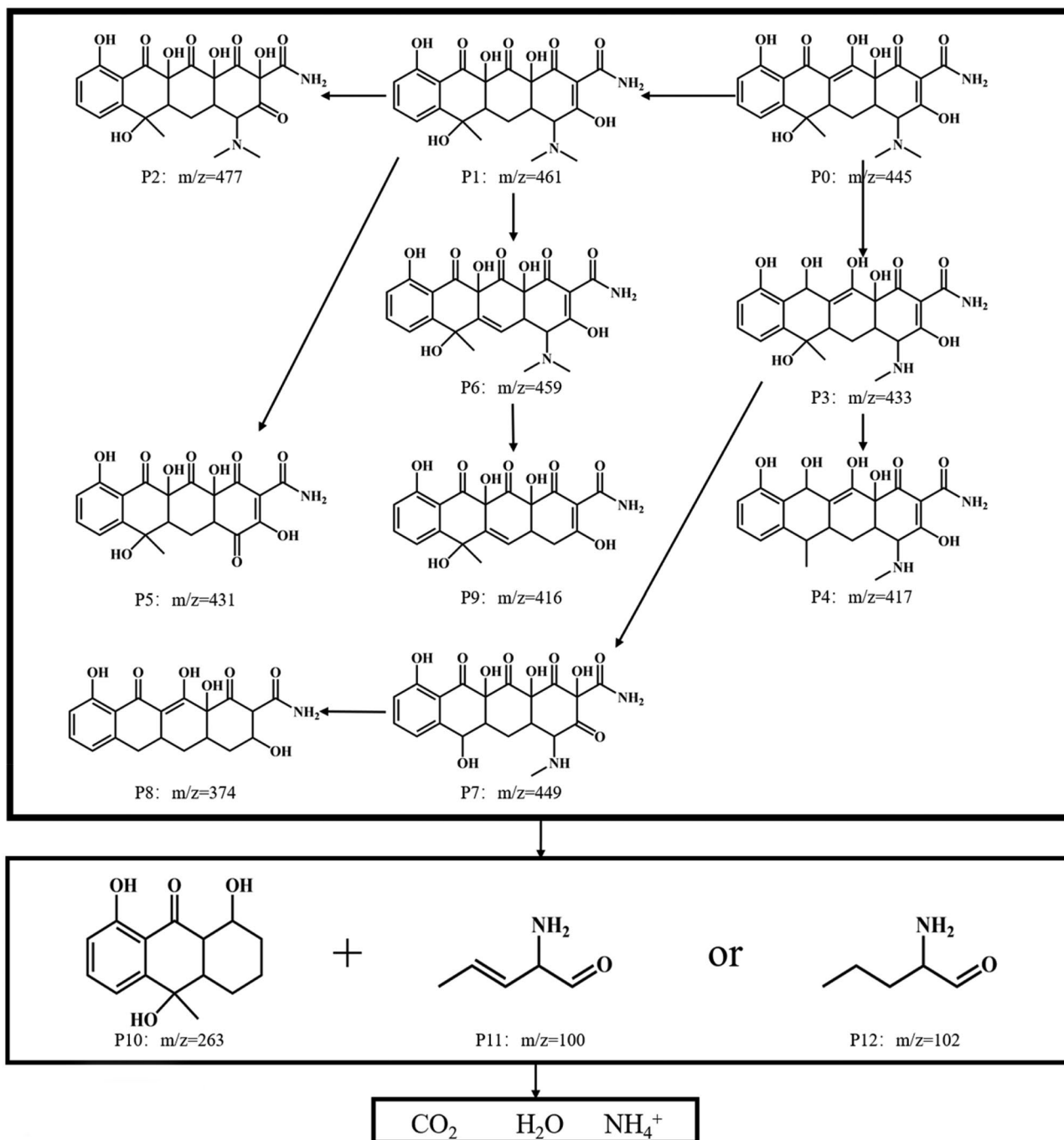


Fig. 6 Proposed pathways for the electrocatalytic degradation of tetracycline by Fe/Co-CNFs

further break of remaining ring structures. Unfortunately, the subsequent products are hardly detected in the chromatograms due to the limit of instrument. In consideration of HPLC result in Fig. 5F and TOC results, the TC molecule is confirmed to be completely mineralized into carbon dioxide and water after the electrocatalytic degradation by LCMO/CNF-modified electrode.

4 Conclusions

In conclusion, a new kind of electrocatalyst comprised of $\text{La}_{0.67}\text{Ca}_{0.33}\text{MnO}_3$ nanoparticles on the carbon nanofibers (LCMO/CNFs) has been manufactured for the TC degradation. The optimal condition for yielding LCMO/CNFs with an excellent TC degradation performance is that the electrospun

PVP/nitrides nanofibers are put in the tube furnace for annealing at 250 °C of 120 min in the air atmosphere and then calcination at 650 °C of 60 min in the nitrogen condition. The optimal TC electrocatalytic degradation factors for LCMO/CNF-modified electrode is at a bias voltage of 1.0 V (vs. SCE) in the solution with pH value of 5.0 and 0.1 mol L⁻¹ of Na₂SO₄ as supporting electrolyte. LCMO/CNF-modified electrode could eliminate the TC solution with initial concentration of 10 mg L⁻¹ to 94.0% during only 1 h treatment, illustrating a very high efficiency. It also depicts the outstanding recyclability and durability with DP% of TC from 87.8 to 84.8% after five cycles of regeneration and reuse. The electrocatalytic degradation of TC by LCMO/CNF-modified electrode is an exhaustive decomposition process without generating any toxic intermediates. The average power consumption for the complete degradation of TC is only 5.41 kWh kg⁻¹ and the overall Faraday efficiency still reaches 46.37% after a 180 min usage. These LCMO/CNFs are easy to be fabricated and could be potentially applied in the treatment of antibiotic wastewater. Our LCMO/CNFs are a promising electrocatalyst for the degradation of antibiotic wastewater with high efficiency and low cost.

Supplementary Information The online version contains supplementary material available at <https://doi.org/10.1007/s42114-022-00550-y>.

Acknowledgements The authors thank Beijing Zhongkebaice Technology Service Co., Ltd for TEM measurements.

Author contribution H. Gu designed this study. Z. Li and W. Xie performed the experiments and analysis. F. Yao is denoted to Fig. 1. A. Du and Q. Wang contribute to Fig. 4 and Fig. 5. H. Gu and Z. Guo wrote the manuscript. All authors contributed to the discussion and improvement of the manuscript.

Funding This work was funded by the Shanghai Rising-star Program (19QA1409400) and the Fundamental Research Funds for the Central Universities (2022-4-YB-03). This work is also supported by Shanghai Science and Technology Commission (19DZ2271500).

Declarations

Conflict of interest The authors declare no conflict of interests.

References

- Marchant J (2018) When antibiotics turn toxic. *Nature* 555:431–433
- Xin S, Huo S, Zhang C, Ma X, Liu W, Xin Y, Gao M (2022) Coupling nitrogen/oxygen self-doped biomass porous carbon cathode catalyst with CuFeO₂/biochar particle catalyst for the heterogeneous visible-light driven photo-electro-Fenton degradation of tetracycline. *Appl Catal B* 305:121024
- Yang G, Gao Q, Yang S, Yin S, Cai X, Yu X, Zhang S, Fang Y (2020) Strong adsorption of tetracycline hydrochloride on magnetic carbon-coated cobalt oxide nanoparticles. *Chemosphere* 239:124831
- Danish M, Qamar M, Suliman MH, Muneer M (2020) Photo-electrochemical and photocatalytic properties of Fe@ZnSQDs/TiO₂ nanocomposites for degradation of different chromophoric organic pollutants in aqueous suspension. *Adv Compos Hybrid Mater* 3:570–582
- Li X, Yan J, Zhu K (2021) Fabrication and characterization of Pt doped Ti/Sb-SnO₂ electrode and its efficient electro-catalytic activity toward phenol. *Eng Sci* 15:38–46
- Li W, Cao J, Xiong W, Yang Z, Sun S, Jia M, Xu Z (2020) In-situ growing of metal-organic frameworks on three-dimensional iron network as an efficient adsorbent for antibiotics removal. *Chem Eng J* 392:124844
- Ahmadi SAR, Kalaei MR, Moradi O, Nosratinia F, Abdouss M (2021) Core-shell activated carbon-ZIF-8 nanomaterials for the removal of tetracycline from polluted aqueous solution. *Adv Compos Hybrid Mater* 4:1384–1397
- Sun P, Zhou S, Yang Y, Liu S, Cao Q, Wang Y, Wågberg T, Hu G (2022) Artificial chloroplast-like phosphotungstic acid-iron oxide microbox heterojunctions penetrated by carbon nanotubes for solar photocatalytic degradation of tetracycline antibiotics in wastewater. *Adv Compos Hybrid Mater*. <https://doi.org/10.1007/s42114-022-00462-x>
- Martinez-Huitle CA, Panizza M (2018) Electrochemical oxidation of organic pollutants for wastewater treatment. *Curr Opin Electrochem* 11:62–71
- Xie R, Meng X, Sun P, Niu J, Jiang W, Bottomley L, Li D, Chen Y, Crittenden J (2017) Electrochemical oxidation of ofloxacin using a TiO₂-based SnO₂-Sb/polytetrafluoroethylene resin-PbO₂ electrode: Reaction kinetics and mass transfer impact. *Appl Catal B* 203:515–525
- Calixto CMF, Cavalheiro ÉTG (2017) Determination of tetracycline in bovine and breast milk using a graphite-polyurethane composite electrode. *Anal Lett* 50:2323–2334
- Yu M, Yu T, Chen S, Guo Z, Seok I (2020) A facile synthesis of Ag/TiO₂/rGO nanocomposites with enhanced visible light photocatalytic activity. *ES Mater Manuf* 7:64–69
- Duan P, Yang X, Huang G, Wei J, Sun Z, Hu X (2019) La₂O₃-CuO₂/CNTs electrode with excellent electrocatalytic oxidation ability for ceftazidime removal from aqueous solution. *Colloids Surf A* 569:119–128
- Liu Z, Zhu M, Zhao L, Deng C, Ma J, Wang Z, Liu H, Wang H (2017) Aqueous tetracycline degradation by coal-based carbon electrocatalytic filtration membrane: Effect of nano antimony-doped tin dioxide coating. *Chem Eng J* 314:59–68
- Tang B, Du J, Feng Q, Zhang J, Wu D, Jiang X, Dai Y, Zou J (2018) Enhanced generation of hydroxyl radicals on well-crystallized molybdenum trioxide/nano-graphite anode with sesame cake-like structure for degradation of bio-refractory antibiotic. *J Colloid Interface Sci* 517:28–39
- Smitha MG, Murugendrapa MV (2019) Transport and complex modulus study of La_{0.7}Ca_{0.3}MnO₃ perovskite manganite nanocompound with polypyrrole as host. *Polym Bull* 76:5363–5380
- Xia W, Li L, Wu H, Xue P, Zhu X (2017) Structural, morphological, and magnetic properties of sol-gel derived La_{0.7}Ca_{0.3}MnO₃ manganite nanoparticles. *Ceram Int* 43:3274–3283
- Sato W, Komatsuda S, Shimizu H, Moriichi R, Abe S, Watanabe S, Komatsu S, Terai T, Kawata S, Ohkubo Y (2019) Dynamic motion and freezing of polaronic local structures in a colossal-magnetoresistive perovskite manganite La_{0.7}Ca_{0.3}MnO₃ detected with radioactive nuclei. *Phys Rev B* 100:184111
- Wang Y, Xie W, Liu H, Gu H (2020) Hyperelastic magnetic reduced graphene oxide three-dimensional framework with superb oil and organic solvent adsorption capability. *Adv Compos Hybrid Mater* 3:473–484
- Tian S, Zhang Y, Zeng D, Wang H, Li N, Xie C, Pan C, Zhao X (2015) Surface doping of La ions into ZnO nanocrystals to lower

- the optimal working temperature for HCHO sensing properties. *Phys Chem Chem Phys* 17:27437–27445
21. Canepa P, Ghiara G, Spotorno R, Canepa M, Cavalleri O (2021) Structural vs. electrochemical investigation of niobium oxide layers anodically grown in a Ca and P containing electrolyte. *J Alloys Compd* 851:156937
 22. Shih Y-J, Chen Y-R, Chen C-L, Lin J-Y, Huang C-P (2021) The electroadsorption characteristics of simple aqueous ions on loofah-derived activated carbon decorated with manganese dioxide polymorphs: the effect of pseudocapacitance and beyond. *Chem Eng J* 425:130606
 23. Pang Y, Zhou X, Vovk EI, Guan C, Li S, van Bavel AP, Yang Y (2021) Understanding lanthanum oxide surface structure by DFT simulation of oxygen 1s calibrated binding energy in XPS after in situ treatment. *Appl Surf Sci* 548:149214
 24. Cai J, Wang W, Xie W, Wei X, Liu H, Wei S, Gu H, Guo Z (2020) Carbon microfibers with tailored surface functionalities supporting iron/nickel bisalloy for highly efficient hexavalent chromium recovery. *Carbon* 168:640–649
 25. Xie W, Shi Y, Wang Y, Zheng Y, Liu H, Hu Q, Wei S, Gu H, Guo Z (2021) Electrospun iron/cobalt alloy nanoparticles on carbon nanofibers towards exhaustive electrocatalytic degradation of tetracycline in wastewater. *Chem Eng J* 405:126585
 26. Xie TT, Hu HT, Chen DH, Sun PZ (2017) Electrochemical degradation of tetracycline hydrochloride in aqueous medium by (B₄C/C)-beta-PbO₂ electrode. *Bull Korean Chem Soc* 38:756–762
 27. Gu H, Xie W, Du A, Pan D, Guo Z (2021) Overview of electrocatalytic treatment of antibiotic pollutants in wastewater. *Catal Rev Sci Eng*. <https://doi.org/10.1080/01614940.01612021.01960009>
 28. Ray SK, Dhakal D, Gyawali G, Joshi B, Koirala AR, Lee SW (2019) Transformation of tetracycline in water during degradation by visible light driven Ag nanoparticles decorated alpha-NiMoO₄ nanorods: Mechanism and pathways. *Chem Eng J* 373:259–274
 29. Sun W, Sun Y, Shah KJ, Chiang P-C, Zheng H (2019) Electrocatalytic oxidation of tetracycline by Bi-Sn-Sb/ γ -Al₂O₃ three-dimensional particle electrode. *J Hazard Mater* 370:24–32
 30. Zheng J, Fan C, Li X, Yang Q, Wang D, Duan A, Ding J, Rong S, Chen Z, Luo J, Zhang B (2022) Enhanced photodegradation of tetracycline hydrochloride by hexameric AgBr/Zn-Al MMO S-scheme heterojunction photocatalysts: Low metal leaching, degradation mechanism and intermediates. *Chem Eng J* 446:137371
 31. Zhang TH, Liu YJ, Rao YD, Li XP, Yuan DL, Tang SF, Zhao QX (2020) Enhanced photocatalytic activity of TiO₂ with acetylene black and persulfate for degradation of tetracycline hydrochloride under visible light. *Chem Eng J* 384:10
 32. Qu Z, Jing Z, Chen X, Wang Z, Ren H, Huang L (2023) Preparation and photocatalytic performance study of dual Z-scheme Bi₂Zr₂O₇/g-C₃N₄/Ag₃PO₄ for removal of antibiotics by visible-light. *J Environ Sci* 125:349–361
 33. Luo T, Feng H, Tang L, Lu Y, Tang W, Chen S, Yu J, Xie Q, Ouyang X, Chen Z (2020) Efficient degradation of tetracycline by heterogeneous electro-Fenton process using Cu-doped Fe@Fe₂O₃: mechanism and degradation pathway. *Chem Eng J* 382:122970
 34. Dong HR, Jiang Z, Zhang C, Deng JM, Hou KJ, Cheng YJ, Zhang LH, Zeng GM (2018) Removal of tetracycline by Fe/Ni bimetallic nanoparticles in aqueous solution. *J Colloid Interface Sci* 513:117–125

Publisher's Note Springer Nature remains neutral with regard to jurisdictional claims in published maps and institutional affiliations.

Springer Nature or its licensor holds exclusive rights to this article under a publishing agreement with the author(s) or other rightsholder(s); author self-archiving of the accepted manuscript version of this article is solely governed by the terms of such publishing agreement and applicable law.